

## Ultimate load behavior of horizontally curved composite plate girders

N. E. Shanmugam\*, M. A. Basher and A. R. Khalim

*Department of Civil and Structural Engineering, University Kebangsaan Malaysia, 43600 UKM Bangi, Selangor Darul Ehsan, Malaysia*

*(Received October 10, 2008, Accepted April 16, 2009)*

**Abstract.** This paper is concerned with steel-concrete composite plate girders curved in plan. At the design stage these girders are assumed sometimes to act independent of the deck slabs resting on them in order to simplify the analysis. The advantage of composite action between the steel girders and concrete deck is not utilized. Finite element modeling of such composite action in plate girders is considered in this paper. Details of the finite element modeling and the non-linear analysis of the girders are presented along with the results obtained. Tension field action in the web panels similar to those observed in the straight plate girders is also noticed in these girders. Finite element and experimental results in respect of curved steel plate girders and straight composite plate girders tested by other researchers are presented first to assess the accuracy of the modeling. Effects of parameters such as curvature, steel flange width and web panel width that affect the behavior of composite girders are then considered in the analyses. An approximate method to predict the ultimate strength of horizontally curved composite plate girders is also presented.

**Keywords :** composite plate girders; horizontally curved; ultimate shear strength; tension field; finite element method.

---

### 1. Introduction

Plate girders curved in plan are frequently employed in the construction of modern highway bridges (Hall 1996). Though the use of continuous curved girders has many advantages over conventional ways of using series of straight chords to form the curved alignment, engineers were reluctant to use them because of mathematical complexities associated with the analysis of such girder systems. The capacity of curved girders to resist external loads is notably decreased due to the existence of the initial curvature. As the curvature increases, excessive deflections may occur. Such deflections are caused by the tendency to include more vertical and rotational rigid body motion in the displacement field. The vertical displacement and the rotation are not independent but coupled in the horizontally curved beams. The rotation is often restrained by providing lateral supports such as cross frames, diaphragms, and bracings connecting two or more parallel girders, which also leads to significant reduction of the vertical displacement. The complex behavior can be easily investigated and accounted for in design using today's powerful digital computers and advanced software. Designers at the preliminary stage assume sometimes that these girders act independent of the deck slabs resting on them in order to

\* Professor, Corresponding Author, Email: [neshanmugam@yahoo.com](mailto:neshanmugam@yahoo.com)

simplify the analysis. The advantage of composite action between the steel girders and concrete deck is not considered. The present study is concerned with such composite action in horizontally curved girders.

An experimental investigation on full-scale horizontally curved steel plate girders has been carried out by Zureick, *et al.* (2002) to study their overall behavior and to determine the shear strength. Web plate slenderness ( $d/t$ ) approximately equal to the largest value permitted for transversely stiffened members by the American Association of State Highway and Transportation Officials (AASHTO) (2004) and panel aspect ratio  $b/d = 1.5$  and  $3.0$  were tested to study the influence of horizontal curvature on the post-buckling shear response. Shanmugam, *et al.* (2003) tested medium size plate girders curved in plan to investigate the ultimate load behavior and load carrying capacity. Finite element modeling of the girders was also proposed. Web openings may need to be provided in these structural members. Lian and Shanmugam (2003) carried out experimental and finite element studies on horizontally curved plate girders containing centrally located circular web openings.

Extensive studies considering parameters such as shear force at the opening, bending moment at the center-line of the opening, slenderness of the web  $d/t$ , web aspect ratio  $b/d$ , size of the hole relative to depth of the web  $d_o/d$ , stiffness of the flange and of the T-section above and below the hole, presence of any reinforcement around the opening and degree of curvature of the curved girder have been carried out and simple design method proposed (Lian and Shanmugam 2004). Jung and White (2006) have reported recently results obtained from the finite element analyses of full-scale curved girders tested by Zureick, *et al.* (2002). Both the elastic shear buckling and full nonlinear maximum shear strength responses have been considered. Effects of parameters such as residual stresses, geometric imperfections and flange size were considered in the analyses and, results on shear strength response, similarities between curved I girders and equivalent straight girders and moment-shear interaction within curved I-girders have been included.

Slender steel-concrete composite plate girders are used extensively for the construction of short and medium span bridges (Lääne and Lebet 2005). The advantage of composite action between plate girders and concrete slab has been investigated in the early eighties in respect of straight girders. Allison, *et al.* (1982) carried out an experimental investigation on steel-concrete composite plate girders under combined shear and negative bending. One steel and five composite plate girders having a fixed web-depth to thickness ( $d/t$ ) ratio of 130 were tested. Based on the experimental results and on the analytical model by Porter, *et al.* (1975) and Evans, *et al.* (1978) to predict the ultimate load-carrying capacity of plate girders, Allison, *et al.* (1982) proposed equations to determine the collapse load of composite plate girders.

The effects of combined shear and bending on composite plate girders were investigated recently both experimentally and numerically (Baskar and Shanmugam 2003, Shanmugam and Baskar 2003, 2006). Finite element modeling was proposed, parametric studies carried out and design method to determine the shear capacity given. However, no detailed study, experimental or analytical, could be found in the literature on horizontally curved composite plate girders. The only analytical model reported by Bradford, *et al.* (2001) deals with the structural behavior of unpropped composite I-section girders curved in plan during construction when composite action between steel and concrete has not been achieved. It has been reported that the load carrying capacities of composite curved girders decrease rapidly as the included angle increases. For curved beams with an included angle  $1^\circ < \theta < 20^\circ$ , both bending and torsion become important. The web buckling is not considered in this analysis.

The current paper is concerned with horizontally curved composite plate girders in which the behavior and load carrying capacity are predominantly governed by tension field action in the web panels. Finite element method has been used to investigate the elastic and ultimate load behavior.

Results are presented to show the effects of transverse stiffener spacing, radius of curvature and flange size on the ultimate strength. Details of the finite element modeling and the results obtained from the analyses are presented herein. Also, an approximate method to predict the ultimate shear strength of horizontally curved composite plate girders is presented.

## 2. Finite element analysis

Finite element software LUSAS version 13.7 has been used in the analysis presented in this paper. Three-dimensional models were developed by idealizing the flange, web, and stiffener plates in plate girders using QSL8 thin shell element in the LUSAS element library (FEA Ltd. 2003). This element allows for buckling and second order effects in the plated structures such as those considered in the present study. Steel plate girders were modelled using ungraded Mild Steel with Young's Modulus equal to  $209 \text{ kN/mm}^2$  and Poisson's ratio of 0.3. The nonlinear material model used Von Mises yield criterion, an associated flow rule and isotropic hardening, giving three distinct regimes - elastic, perfectly plastic and multi-linear strain hardening respectively.

Concrete slab was idealized by three dimensional hexahedral isoparametric solid continuum elements (HX20) with higher order models capable of modeling curved boundaries. This solid element has 20 nodes with three degrees of freedom at each node representing the three global directions in which it may move. The concrete material properties adopted in LUSAS has been obtained from uniaxial stress-strain curves in tension and compression as shown in Fig. 1. In the analyses, compressive strength ( $f_c$ ) equal to  $35 \text{ N/mm}^2$ , tensile strength ( $f_t$ ) of  $3.92 \text{ N/mm}^2$ , compressive strain ( $\epsilon_c$ ) of 0.003, tensile strain ( $\epsilon_t$ ) equal to 0.004, Young's Modulus of  $24 \text{ kN/mm}^2$  and Poisson's ratio of 0.2 have been assumed.

Also, in LUSAS, a new multiple non-orthogonal cracking concrete model has been implemented for plane stress, plane strain, axisymmetric and 3D solid analysis. This model may be used to represent the nonlinear material effects associated with the cracking of concrete. The multi crack model assumes that, at any one material point, there are a pre defined number of permissible crack directions. This is set to 21 for 3D, 8 for plane stress and 9 for plane strain and axisymmetric. Each direction defines a possible cracking plane and for each of these planes there is a separate yield surface and set of yield state variables. Only 3 active (open or opening) cracks (2 for plane stress), closest to the principal strain directions, are permitted at any one time. In the compression-compression region the material is assumed to behave elastically (i.e. no crushing is allowed).

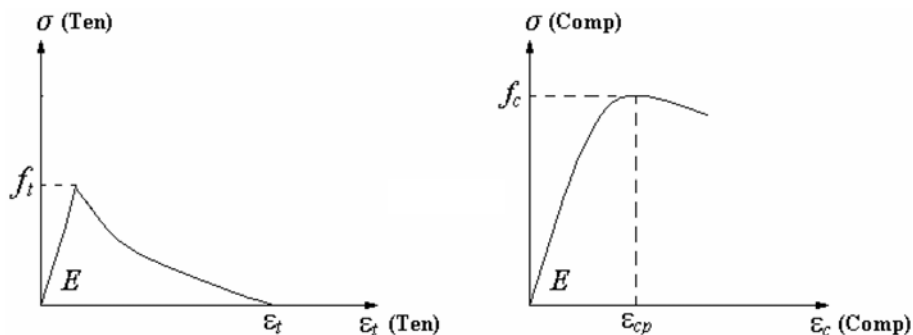


Fig. 1 Stress-strain behavior in concrete

A perfectly straight and un-deformed model would provide different answers from a model with imperfect geometry. In LUSAS an imperfection can be built into the initial model by manually defining the appropriate geometry or it can be arrived at by loading a previous results file, selecting the load case of interest and choosing the LUSAS Data file command and selecting the deformed mesh factor option to create a model having deformed geometry appropriate to the eigenvalue or load case chosen. In this study, the initial imperfection of the modelled girders was obtained from the buckling analysis whereby the deformed mesh from the first eigenvalue was used for the nonlinear analysis. Crisfield's arc length control is used in this study as it enhances convergence of the increment after the solution reaching limit point.

Regular mesh with element size of 80 mm × 80 mm resulting in 14572 elements was adopted in the analyses as per the definition in the Attributes options tabs in LUSAS. A typical mesh used in all the analyses is shown in Fig. 2 and, it was chosen based on convergence studies carried out to determine the optimal mesh that gives a relatively accurate solution and one that takes low computational time. An example of the convergence studies carried out for the girder C1 is shown in Fig. 3. It has been found that the mesh chosen is capable of producing results close to the actual behavior of the girder. With large number of elements a more accurate value can be obtained, but the computation time will be longer.

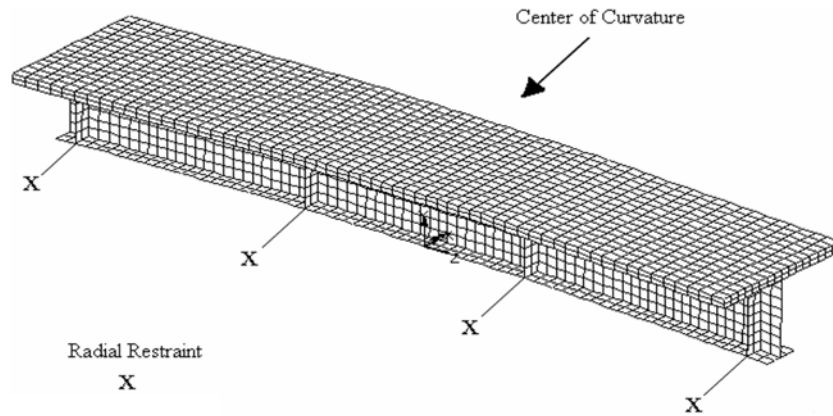


Fig. 2 Typical finite element modelling used in the analyses

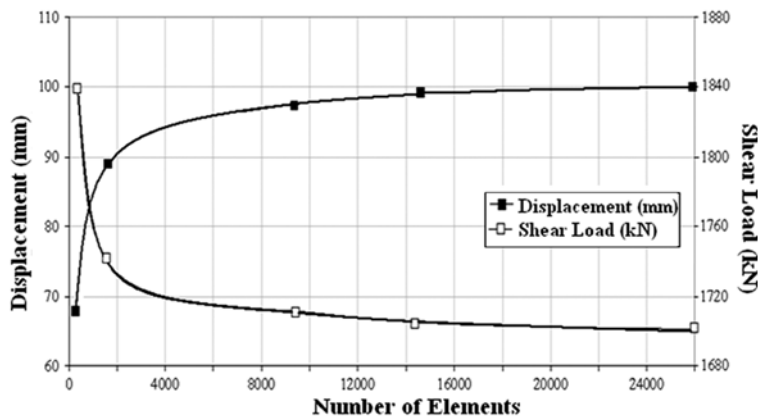


Fig. 3 Convergence study for the girder C1

### 3. Accuracy of the finite element modeling

It is important to establish the accuracy of the finite element modeling before undertaking the analysis of horizontally curved composite plate girders. Neither experimental nor analytical results could be found for comparison in the literature for composite plate girders curved in plan. Horizontally curved steel plate girder tested by Zureick, *et al.* (2002) and straight composite plate girders tested by Shanmugam and Baskar (2003) were, therefore, considered for comparison and to assess the finite element modeling using LUSAS. Finite element modeling was made and analyses carried out to study the elastic and ultimate load behaviour of typical girders.

#### 3.1 Horizontally curved steel plate girders

Zureick, *et al.* (2002) carried out full-scale tests on four steel plate girders identified in the text as S1, S2, S1-S and S2-S of 11.58 m chord length. Transverse stiffeners along the girder length were positioned such that the panel aspect ratio was 3 in the case of S1 and S2 and 1.5 in the case of S1-S and S2-S. The overall depth of the girders was around 1.22 m whilst the top and bottom flanges of around 22.9 mm thick varied in width from 546.6 mm as in the case of S1 and S1-S and, 556.3 mm for S2 and S2-S. Web slenderness ( $D/t_w$ ) in all the four girders was kept 154, approximately equal to the minimum value of 150 permitted for transversely stiffened plate girders by AASHTO (2004). The flange slenderness ( $b_f/2t_f$ ) varied between 11.92 and 12.19. The girders S1 and S1-S had a nominal radius of 63.63 m whilst the corresponding value for the girders S2 and S2-S was 36.58 m. The cross-sectional dimensions of the girders are shown in Fig. 4 and the overall geometry of the test girders in Fig. 5. Test set-up and applied loading in the tests are shown in Fig. 6. Also shown in Fig. 6 are shear force and bending moment diagrams corresponding to the applied loading.

Further details of the test girders may be found in the reference by Jung and White (2006). Typical girders S2 and S2-S were analyzed using LUSAS and the finite element mesh shown in Fig. 2 in order to establish the accuracy of the finite element modeling. Load-deflection plots in respect of the girders are shown in Figs. 7 and 8. In the figures, experimental results along with the ABAQUS results given by Jung and White (2006) are also plotted for comparison. It can be seen from the figures that the load-deflection plots obtained from the analyses by LUSAS lie close to the corresponding experimental and

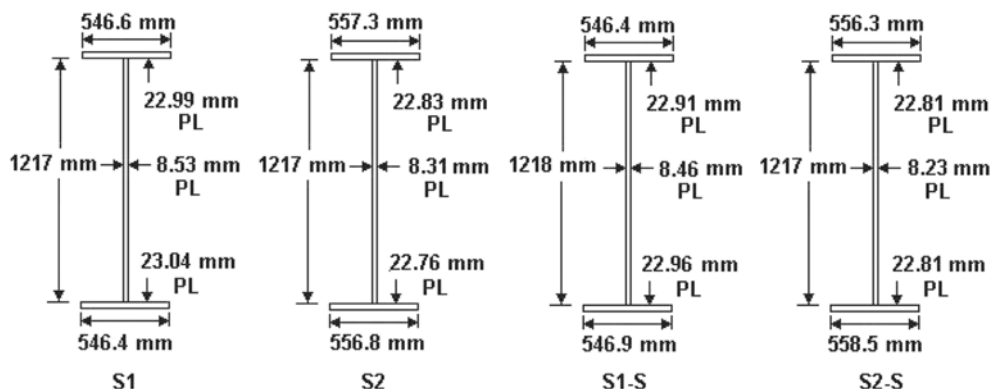


Fig. 4 Cross-sectional dimensions of the test girders by Zureick, *et al.* (2002)

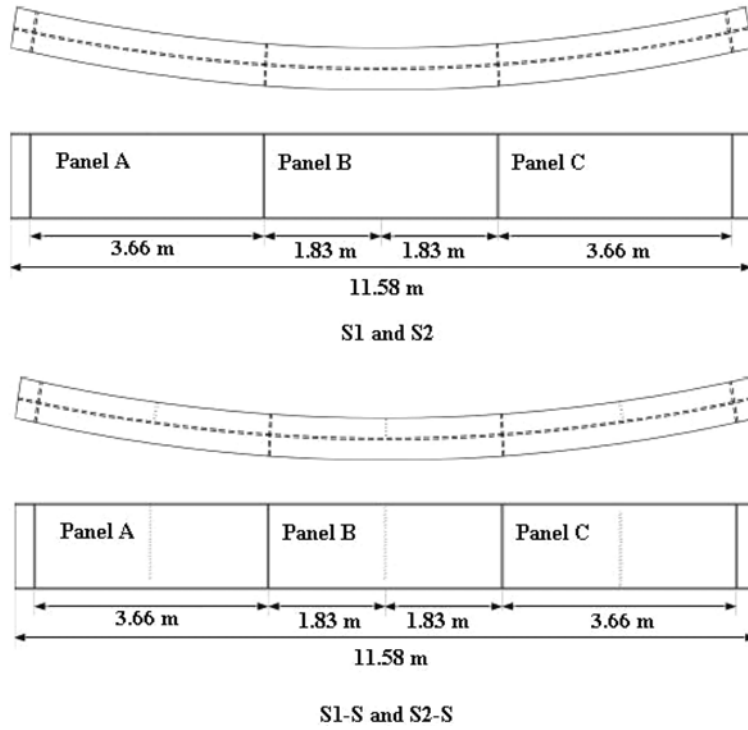


Fig. 5 Overall geometry of the test girders (Jung and White 2006)

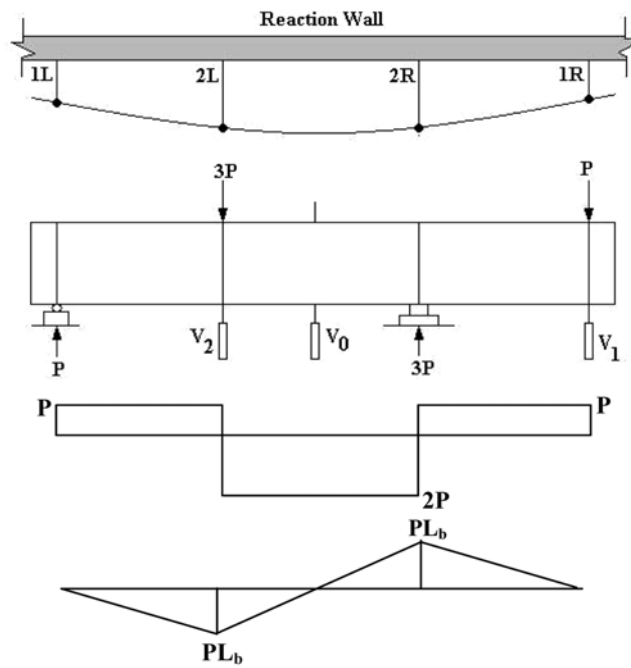


Fig. 6 Test set-up and applied loading (Jung and White 2006)

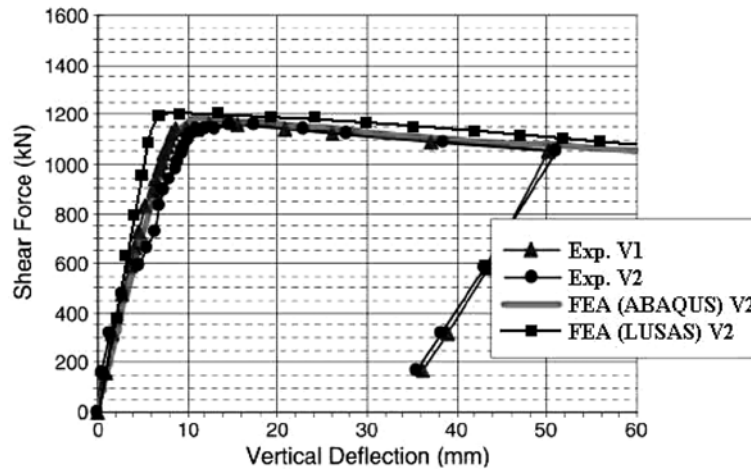


Fig. 7 Load-deflection plots for steel girder S2 tested by Zureick, *et al.* (2002)

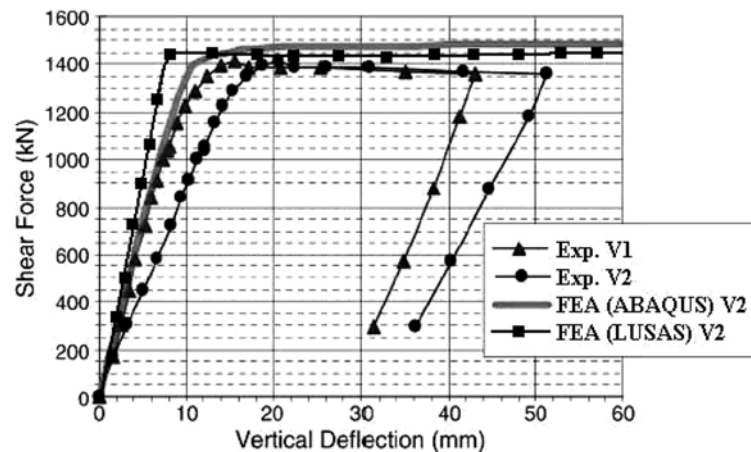


Fig. 8 Load-deflection plots for steel girder S2-S tested by Zureick, *et al.* (2002)

ABAQUS curves thus establishing the accuracy of the computer package LUSAS. However, initial slope of the load-deflection plots in respect of S2-S deviate slightly from each other and, small difference exists between the two sets of results in this case. This may be due to differences in the LUSAS and ABAQUS modeling with respect to the experimental model details.

### 3.2 Straight composite plate girders

Studies similar to the above were carried out on straight composite plate girders by Shanmugam and Baskar (2003). Ten medium-scale composite girders were tested to failure and, the results were presented along with those obtained from finite element analyses using ABAQUS. These girders are identified in the text as CPG1 to CPG10. The tests were carried out in two phases; in the first phase, girders were subject to shear loading and in the second phase to the combined action of shear and bending.

Two different web-depth to thickness ( $d/t$ ) ratios viz. 250 and 150 and two different moment/shear ratios were considered. 3 mm thick web plate was chosen for girders with  $d/t$  ratio of 250 and, 5mm thick web plate for girders with  $d/t$  ratio 150. The panel aspect ratio of the web was restricted to 1.5 in all girders. In all composite girders the bond between steel girder and deck slab was achieved by means of shear studs, 19 mm dia, 100 mm long, welded in two rows. The width of deck slab was taken as 1,000 mm with an overall depth of 200 mm. The slab width was 1,200 mm in some girders. The plate slenderness ratio of the flange outstands in steel girders varied from 5 to 6.67. A few of these girders were analyzed using LUSAS and the corresponding load-deflection plots are given along with the experimental results in Figs. 9(a) and 9(b). It can be seen from the figures that LUSAS predictions for ultimate load lie close to the experimental results (maximum deviation being around 8.3%) thus proving the validity of the LUSAS analyses of straight composite plate girders. However, there are minor differences, as seen in the figures, between the experimental and LUSAS predictions of the load-deflection behavior and, it may be attributed to the approximations in the finite element idealization of the physical model.

The results given above in respect of horizontally curved steel plate girder and straight composite girders establish the accuracy of the finite element modeling using LUSAS and the ability of the analyses to account for the horizontal curvature as well as the composite action between the concrete slab and steel plate girders. Having thus established the accuracy of the modeling using LUSAS it was decided to use the computer package for the analyses of horizontally curved composite plate girders.

#### 4. Analysis of horizontally curved composite plate girders

The four steel plate girders, S1, S2, S1-S and S2-S tested by Zureick, *et al.* (2002) were taken as the steel part of the composite girders analyzed in this study. To each of these four steel girders, concrete slab of 200 mm thick and 2,400 mm wide was added at the top flange to act compositely with the steel part. The dimensions of the slab were chosen as per AASHTO recommendations for a composite girder. Full interaction in the composite action was assumed. The resulting four composite girders are

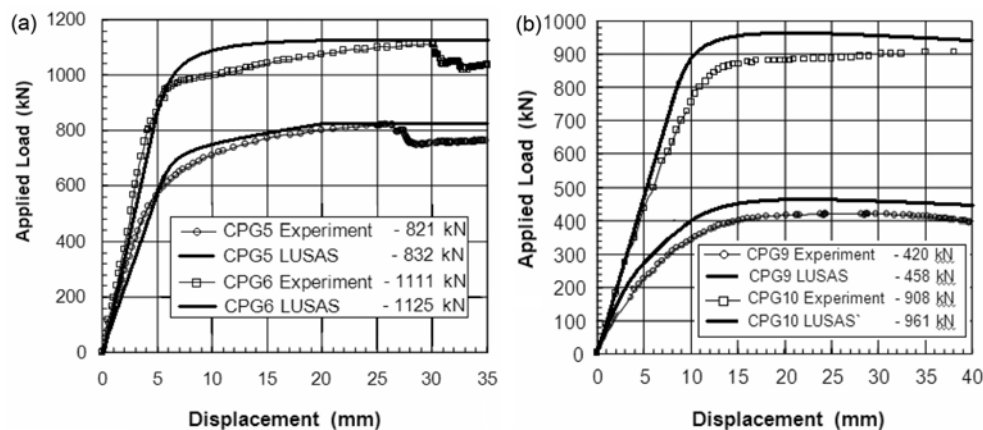


Fig. 9(a) Load deflection plots for CPG5 and CPG6 (Baskar and Shanmugam 2003), (b) Load deflection plots for CPG9 and CPG10 (Baskar and Shanmugam 2003)

identified herein in the text as C1, C2, C1-C and C2-C corresponding to S1, S2, S1-S and S2-S, respectively.

#### 4.1 Description of the composite girders

Girder C1 corresponds to the steel girder S1 tested originally by Zureick, *et al.* (2002) to examine the shear strength of a curved web panel of aspect ratio equal to 3. The ratio the web panel length to the radius of curvature was kept as 0.0575; subtended angle of 0.0575 between the cross frame locations, slightly greater than one-half of the maximum value of 0.1 permitted by AASHTO in the unified provisions for design of straight and curved I-girders was adopted (Jung and White 2006). There were only four bearing stiffeners and no intermediate stiffeners were provided. Concrete slab of 200 mm thick and 2,400 mm wide was added to the steel girder. Girder C1-C was identical to C1 but had an additional intermediate stiffener located at the center of each panel between bearing stiffeners. The resulting web panel ratio in this case was, therefore, equal to 1.5. Girder C2 was similar to C1 but differed only in the radius as 36.58 m thus giving a panel length to radius of curvature ratio of about 0.1. This value is close to the AASHTO requirement  $L_b / R \leq 0.10$ . Girder C2 - C was identical to C1 - C but had a radius of 36.58 m and panel aspect ratio of 1.5. Fig. 10 (a) shows the cross-section of a typical composite girder. A detailed finite element modeling was prepared for each of the girders; the finite element mesh of a typical girder is shown in Fig. 10 (b). The types of elements used for steel part of the girder and for concrete slab are same as those described earlier in this paper.

The support and loading conditions adopted for the analyses of composite girders are same as those used for steel girders by Zureick, *et al.* (2002) and shown in Fig. 6. The vertical support conditions

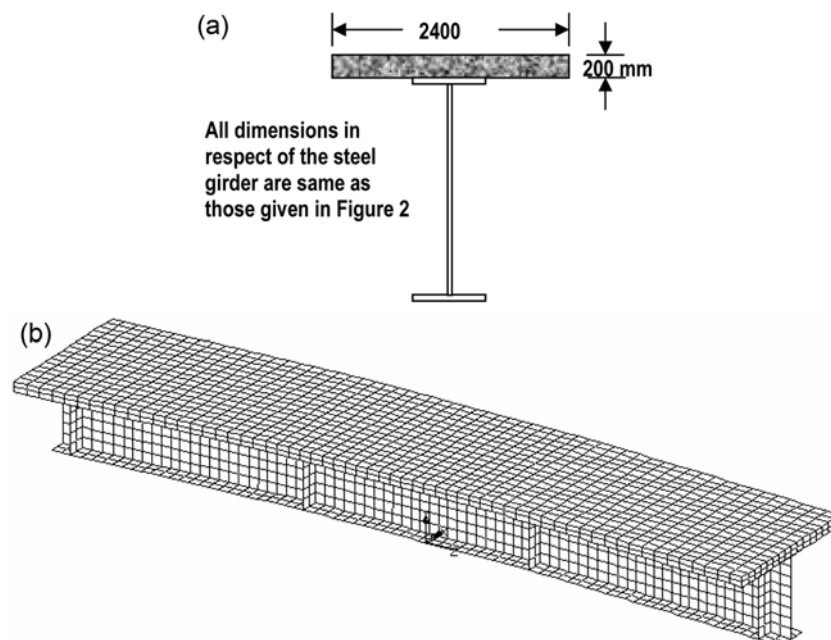


Fig. 10 (a) Cross-section of composite girders, (b) Typical finite element mesh for composite girders

provided for the physical model have been simulated by restraining the corresponding displacements at the nodes along a line across the width of the bottom flange. At the roller support, the girders were free to move along the tangential direction. Suitable restraints by means of truss elements were provided to the girder corresponding to the tube braces used to prevent the lateral torsional buckling of the girders as shown by 1L, 1R, 2L and 2R in Fig. 6. Concentrated loads 3P and P as shown in Fig. 4 were simulated in the analyses by means of displacement control. Nominal residual stresses and imperfections for the steel part of the girder have been assumed in the analyses. The results obtained from the finite element analyses using LUSAS for all the four girders are presented in the following sections.

#### 4.2 Results and discussion

The finite element analyses provided detailed output in terms of displacements, stresses, strains, moments and forces. However, for brevity only the most relevant results are presented herein for discussion. Figs. 11-14 show the load-vertical deflection plots for the four girders. Deflection measured at the center of the supported span ( $V_2$ ) is plotted against the corresponding shear force (P). In these figures, results corresponding to steel girders (Jung and white 2006) are presented along with those for composite girders for comparison.

An elastic behavior at the initial stages is observed for all the girders and it becomes nonlinear soon after reaching the ultimate condition. The behavior of the composite girders is similar to that of the steel girders and enhancement in stiffness and ultimate load-carrying capacity compared to steel girders can be witnessed in all the composite girders. Composite girders exhibit significant gain in the ultimate load capacity, ranging from 28% to 30% over the corresponding values for steel girders. The gain should be attributed to the contribution by the presence of concrete slab and the composite action. There is some increase in stiffness in respect of the girders C1, C1-C and C2 in particular though not significant, as shown in Figs. 11-13.

In Figs. 15 to 18 plotted are radial displacements measured at the mid-depth of the central panel against the shear force at the panel. In each of the figures variation of radial displacements corresponding to the respective steel girders (Jung and White 2006) is also presented for comparison. It can be seen again that behavior of the composite girder is stiffer and stronger compared to the corresponding steel girders.

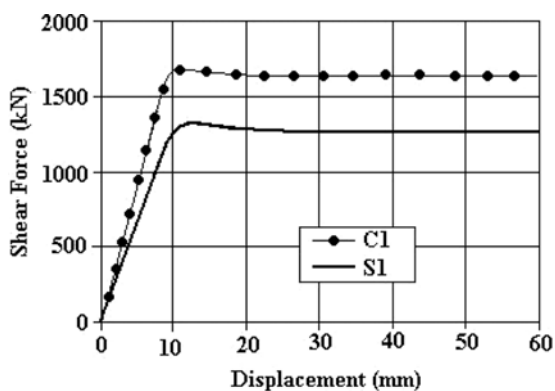


Fig. 11 Load-deflection plot for the girder C1

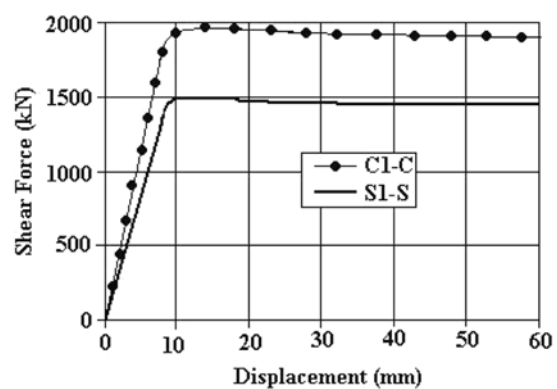


Fig. 12 Load-deflection plot for the girder C1-C

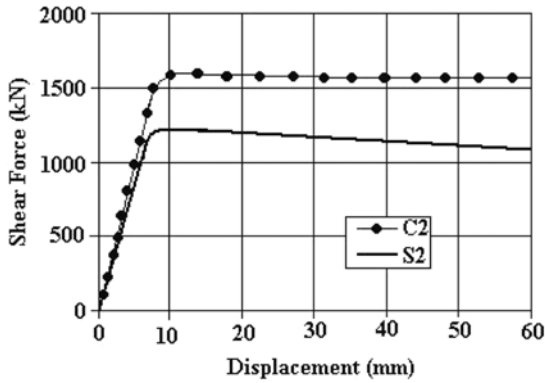


Fig. 13 Load-deflection plot for the girder C2

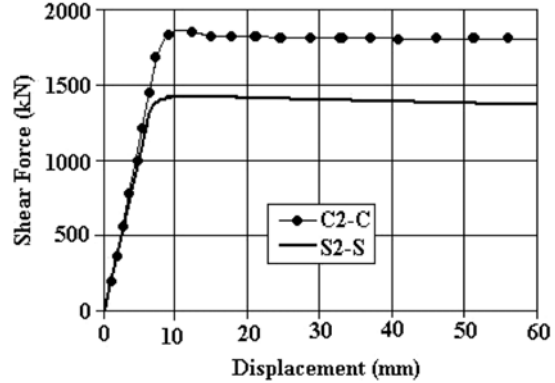


Fig. 14 Load-deflection plot for the girder C2 - C

After the onset of buckling in web panels the girder continues to carry larger load. As the load is increased hence the shear in the webs, out-of-plane deformations continue to grow. Tension field action in the web panels experiencing larger shear force sets in and, it grows further with the increase in load. Fig. 19(a) shows such tension field in the composite girder C1 in which the middle panel subject to larger shear force developed tension field first followed by the outer panels. The figure shows two views of the girder, one corresponding to the state soon after reaching the failure load and the other well beyond the failure load. The middle web panel under larger shear appears to have suffered extensive buckling soon after reaching the failure load. As the displacement is increased beyond the failure load, the adjacent web panels are subject to larger deformation, conspicuous from the deflected shape of the web panels as shown in the figure. Load beyond the ultimate condition leads gradually to collapse of the girder.

Fig. 19(b) shows similar views of tension field in the girder C1-C. Once again it can be seen that the web panel under larger shear suffers buckling initially and other panels buckling under

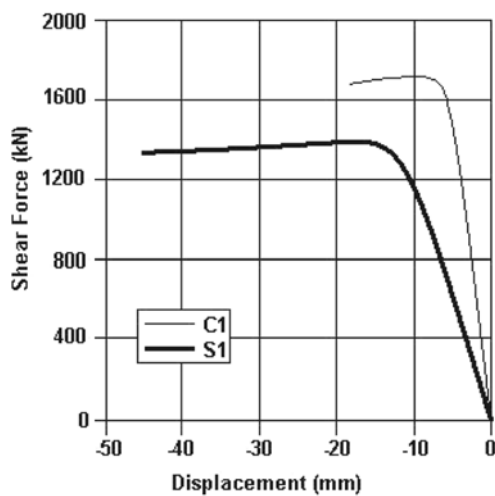


Fig. 15 Radial deflection for C1 and S1

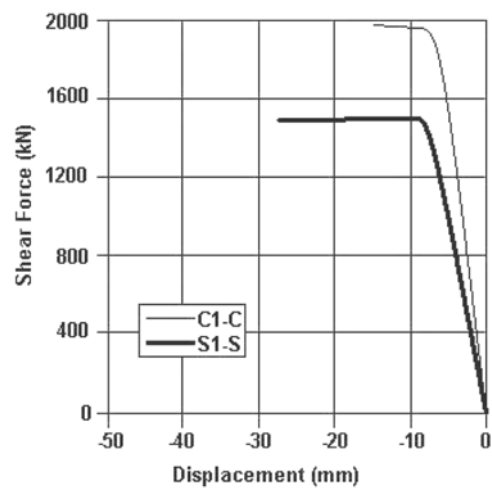


Fig. 16 Radial deflection for C1-C and S1-S

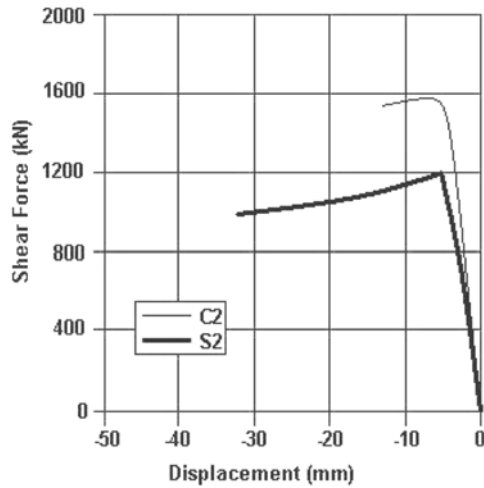


Fig. 17 Radial deflection for C2 and S2

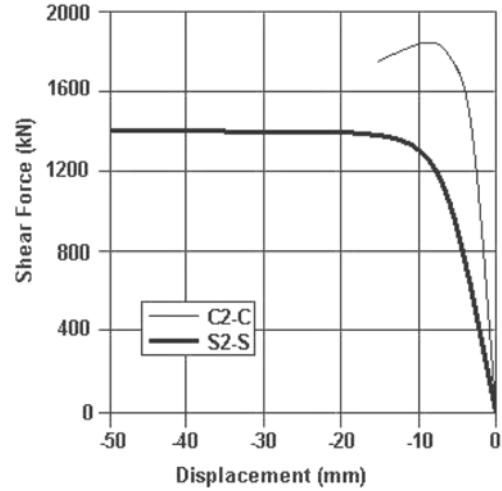


Fig. 18 Radial deflection for C2-C and S2-S

subsequent increase in load or further displacement beyond the failure load. In the girder C1-C the transverse stiffeners are spaced closer than that in the girder C1 and the load resistance increased correspondingly. Since the top flange was restrained by concrete slab no buckling could be noticed in the flange except that the flanges bent due to excessive deformations at ultimate load conditions. It should, however, be remembered that full interaction has been assumed between concrete slab and the steel beam and, the behavior could be different under partial interaction conditions.

Fig. 20 shows the load-vertical deflection plots in which the girders having same radius of curvature are grouped together in order to highlight the panel size effect on the behavior of these girders. As stated earlier the radius of curvature for girders C1 and C1-C is 63.63 m and the corresponding value for C2 and C2-C is 36.58 m. Transverse stiffeners in the case of C1 and C2 are spaced at 3.66 m centre to centre whereas in C1-C and C2-C the spacing is closer, 1.83 m. Thus the effect of web panel size is apparent in the figures in which the girders with smaller panel aspect ratio exhibit larger load carrying capacity and slightly stiffer behavior. The ultimate load in the case of girders having closely spaced stiffeners is around 13% to 18% higher than that for the girders with widely spaced transverse stiffeners. This type of behavior is obvious because of the inherent buckling behavior of these panels under shear loading. Similar observations have been made in the steel girders also (Jung and White 2006).

Studies were also carried out to investigate the effect of curvature on the behavior of composite girders. Fig. 21 shows the results obtained from studies on girder C1 in which the radius of curvature was varied from 50 m to 100 m. Results corresponding to a straight composite girder and the girder C1 are also shown in the figure. It is evident from the figure that the curved girders carry less load compared to the straight one and, the drop in load carrying capacity decreases with increase in radius of curvature. For example, the maximum shear at failure for straight girder is 2318 kN and the corresponding value for the girder with radius of curvature equal to 100 m is 2098 kN, a drop of around 10%. The girder with radius curvature of 50 m could carry only 1,578 kN, a drop of around 30% compared to the straight girder.

The composite girder C1 was analysed by changing the flange rigidity in order to examine its effect on ultimate load behavior. Keeping the thickness constant four different values of flange widths viz., 203 mm, 288 mm, 460 mm and 546 mm were considered in the analysis. Load-vertical deflection responses thus

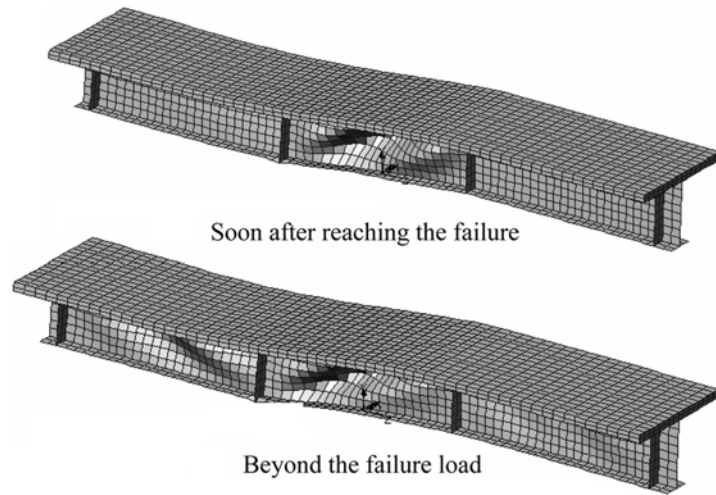


Fig. 19(a) Views after failure of the girder C1

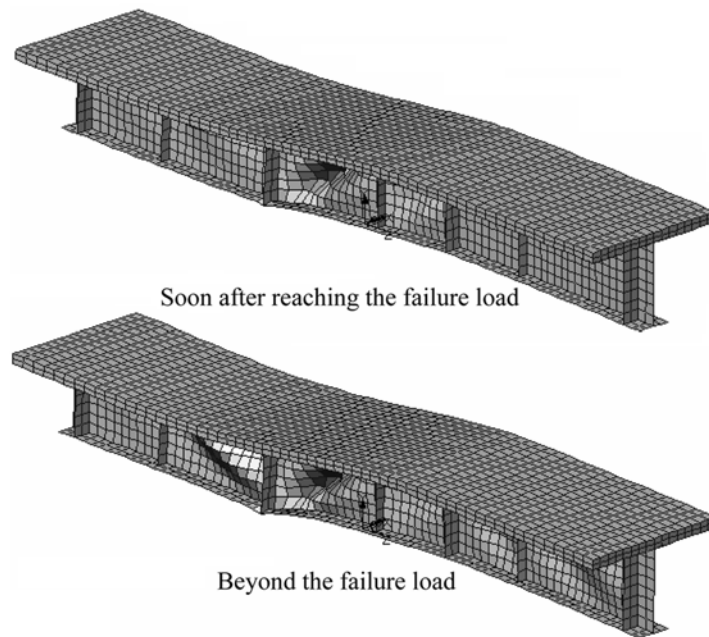


Fig. 19(b) Views after failure of the girder C1-C

obtained are shown Fig. 22. It is obvious from the figure that larger flange width (flange rigidity) results in higher load carrying capacity as expected. The increase in ultimate load is around 25% when the flange width was increased from 203 mm to 546 mm. Care should, however, be exercised to restrict outstand to thickness ratio of the compression flange in order to avoid failure due to local buckling. Larger flange widths do not necessarily result in higher resistance capacity because of flange outstand local buckling in such cases.

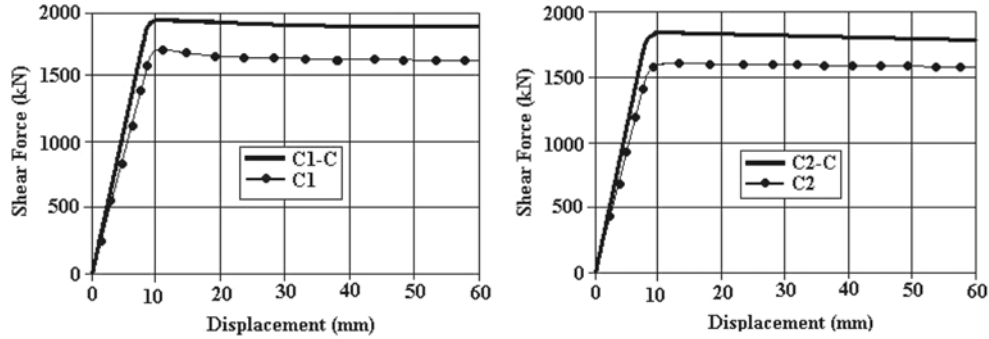


Fig. 20 Panel size effect on the behavior of composite girders

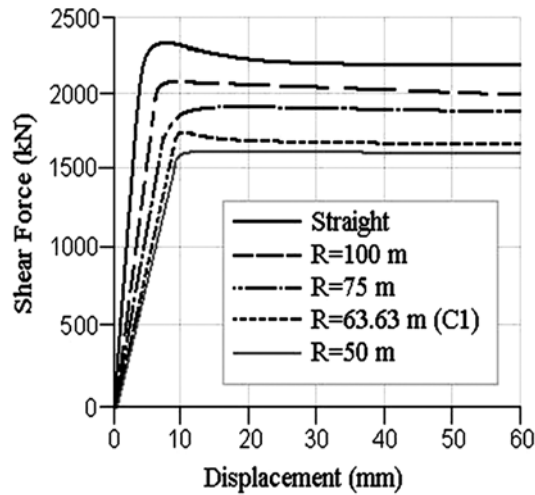


Fig. 21 Effect of radius of curvature on the behavior of composite girders

Design codes impose, therefore, restrictions on width to thickness ratios.

Figs. 23 to 26 show the moment-shear interaction diagrams for the girders C1, C1-C, C2 and C2-C, respectively. Results corresponding to the flange widths, varying from 203.2 mm to 546.6 mm, are presented in these figures. In the analyses with different flange widths, the bearing and intermediate stiffener widths are adjusted to suit the flange dimensions. The maximum shear and moment obtained from the finite element analyses are normalized with respect to nominal shear resistance  $V_n$  and  $M_{n(1/3 \text{ rule})}$  as per the recommendations by AASHTO. The simple equation for major axis bending strength provided by AASHTO accounts for the influence of (or interaction with) flange lateral bending. This equation has been termed as the one-third rule. Nominal shear resistance  $V_n$  is expressed as

$$V_n = V_p \left[ C + \frac{0.87(1-C)}{\left( \sqrt{1 + \left( \frac{d_o}{D} \right)^2} + \frac{d_o}{D} \right)} \right] \quad (1)$$

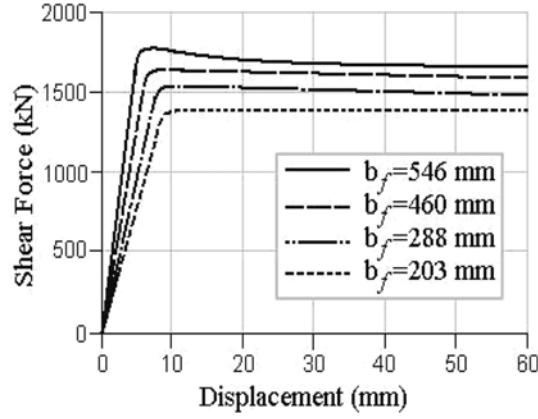


Fig. 22 Effect of flange rigidity on the behavior of composite girders

in which  $V_p$  is the plastic shear force equal to  $0.58F_{yw}Dt_w$ ,  $d_o$  the spacing of stiffeners,  $D$  the web depth and  $C$  the ratio of the shear-buckling resistance to the shear yield strength taken as

$$C = 1.0 \quad \text{if} \quad \frac{D}{t_w} \leq 1.12 \sqrt{\frac{Ek}{F_{yw}}} \quad (2)$$

$$C = \frac{1.12}{\frac{D}{t_w}} \sqrt{\frac{Ek}{F_{yw}}} \quad \text{if} \quad 1.12 \sqrt{\frac{Ek}{F_{yw}}} \leq \frac{D}{t_w} \leq 1.40 \sqrt{\frac{Ek}{F_{yw}}} \quad (3)$$

$$C = \frac{1.57}{\left(\frac{D}{t_w}\right)^2} \left(\frac{Ek}{F_{yw}}\right) \quad \text{if} \quad \frac{D}{t_w} > 1.40 \sqrt{\frac{Ek}{F_{yw}}} \quad (4)$$

Where  $k$  is shear buckling coefficient given as

$$k = 5 + \frac{5}{\left(\frac{d_o}{D}\right)^2} \quad (5)$$

From the finite element results  $V_{\max}$  can be obtained as the maximum shear force and, the maximum moment for each girder is calculated as  $M_{\max} = (V_{\max}/2)L_b$ . The girder flexural strengths per AASHTO in terms of the major-axis bending moment is simply

$$M_{(1/3rule)} = \left(R_b F_{yc} - \frac{f'_c}{3}\right) S_{xc} \quad (6)$$

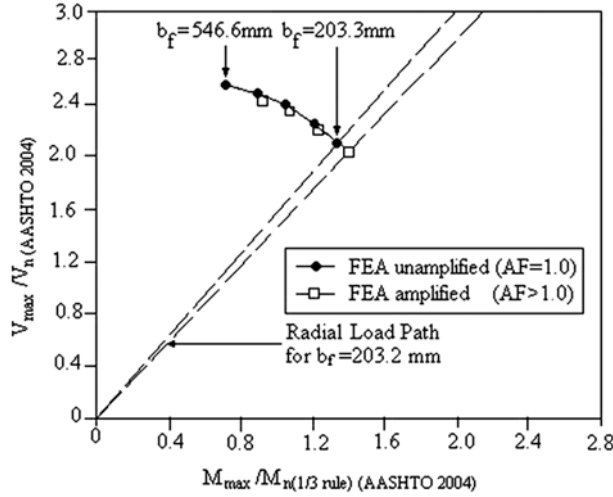


Fig. 23 Moment - shear interaction for the girder C1 with different flange widths

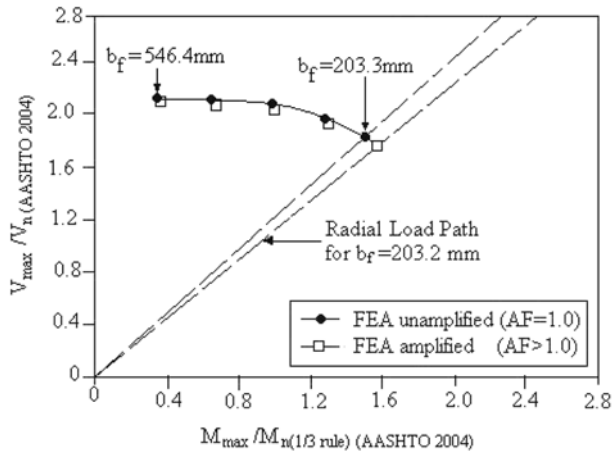


Fig. 24 Moment - shear interaction for the girder C1-C with different flange widths

Where  $R_b$  is the strength reduction factor to account for web post-bend buckling and load shedding effects,  $F_{yc}$  is the compression flange yield strength,  $f_l$  the elastically computed flange lateral bending stress at the maximum load level from the full nonlinear FEA solutions, and  $S_{xc}$  is the elastic section modulus of the composite section to the compression flange. The strength reduction factor can be obtained as

$$R_b = \left( \frac{a_{wc}}{1200 + 300a_{wc}} \right) \left( \frac{2D_c}{t_w} - \lambda_{rw} \right) \leq 1.0 \tag{7}$$

in which  $\lambda_{rw}$  is the limiting slenderness ratio for a web calculated as

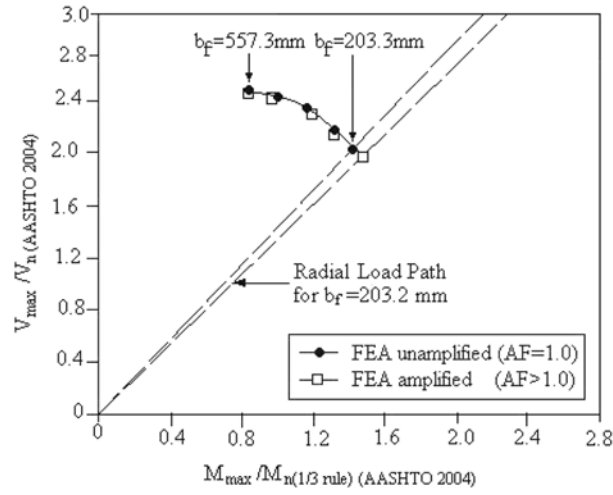


Fig. 25 Moment - shear interaction for the girder C2 with different flange widths

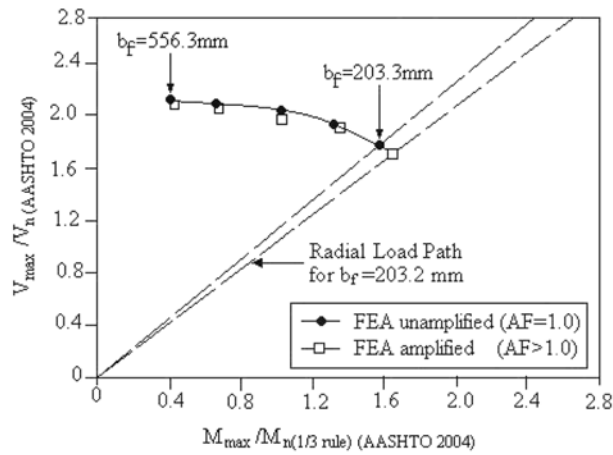


Fig. 26 Moment - shear interaction for the girder C2-C with different flange widths

$$\lambda_{rw} = \sqrt{\frac{E}{F_{yc}}} \quad (8)$$

$$a_{wc} = \frac{2D_c t_w}{b_{fc} t_{fc} + b_s t_s \left(1 - \frac{f_{DC1}}{F_{yc}}\right) \frac{1}{3n}} \quad (9)$$

in which  $b_s$  is the effective width of concrete deck,  $f_{DC1}$  compression flange stress at the section under consideration, calculated without consideration of flange lateral bending and caused by the factored permanent load applied before the concrete deck has hardened or is made composite,  $n$  modular ratio,  $t_s$

the thickness of concrete deck, and  $D_c$  the depth of the web in compression in the elastic range. The flange lateral bending stress may be calculated in general from open-walled section beam theory as

$$f_\ell = \frac{M_\ell \frac{b_f}{2}}{I_{yc}} = \frac{6M_\ell}{b_f t_f} \quad (10)$$

where  $M_\ell$  flange lateral bending moment,  $b_f$  the flange width,  $t_f$  the flange thickness and  $I_{yc}$  the moment of inertia of the individual flanges about a vertical axis through the web.

To illustrate the effect of Amplification Factor (AF), the strengths  $M_n$  (1/3 rule) based on both  $AF > 1.0$  and  $AF = 1$  are included in the results presented in Figs. 23 to 26. AF is calculated as

$$AF = \frac{C_m}{1 - \frac{P}{P_{ek}}} \quad (11)$$

in which  $C_m$  is the equivalent moment factor ( $C_m$  is equal to 1.0 for composite girder),  $P$  factored load, and  $P_{ek}$  the critical elastic buckling.

It can be seen from the figures that the normalized shear capacities ( $V_{max}/V_n$ ) decrease as the flange width is reduced from 546.6 mm to 203.3 mm. This drop is 16.6% in respect of the girder C1, 13.6% for C1-C and around 17% for C2 and C2-C. The nominal shear resistance  $V_n$ , independent of flange width, is not affected by the change in the flange width. It should, therefore, be noted that the variation in normalized shear capacities is entirely due to the drop in the maximum shear developed within the inner panel as a result of reduced flange width. Further observations of Figs. 23 to 26 show that drop in maximum shear capacity  $V_{max}$  due to reduction in flange widths does not show corresponding drop in  $M_{max}/M_{n(1/3 \text{ rule})}$ . In contrast, there is increase in  $M_{max}/M_{n(1/3 \text{ rule})}$  with decrease in flange width.  $M_{max}$  which is equal to  $(V_{max}/2)L_b$  is expected to drop with decrease in flange width as in the case of  $V_{max}$ . The value of  $M_{n(1/3 \text{ rule})}$  is significantly affected by the size of flange width compared to that of  $V_n$  and, the ratio  $M_{max}/M_{n(1/3 \text{ rule})}$  becomes, therefore, considerably large for smaller flange width.

Shear-moment interaction for the girders with the change in flange width appears to be influenced significantly by web panel width as shown in the figures. Comparison of Figs. 23 and 24 shows that the drop in shear capacity, around 16%, occurs with corresponding increase in moment ( $M_{max}/M_{n(1/3 \text{ rule})}$ ) ratio of about 68% in the girder C1 in which the transverse stiffeners are widely spaced ( $b/d = 3.0$ ) whereas the respective values for the girder C1-C with smaller web panel width ( $b/d = 1.5$ ) are around 14% and 300%, respectively. Similar observations could be made in respect of C2 compared to C2-C (Figs. 25 and 26) also. It is seen for all the girders that the  $V_{max}/V_n$  is larger than the ratio  $M_{max}/M_{n(1/3 \text{ rule})}$ . The reduction in  $M_{max}$  calculated as  $(V_{max}/2)L_b$  is small. However, the value of  $M_{n(1/3 \text{ rule})}$ , compared to the value of  $V_n$ , is affected considerably by the flange size. As a result the computed values of  $M_{max}/M_{n(1/3 \text{ rule})}$  ratio is significantly larger for smaller flange widths. It can also be noticed in all cases that the amplification factor has negligible influence on shear-moment interaction behavior.

Views, similar to those shown in Figs. 19 (a) and (b), of the girders with different flange widths show generally that the failure of girders is predominantly governed by web postbuckling shear deformation within the critical web panel. The concrete slab along with steel flange in these girders offered stiff resistance to lateral bending in the compression zone under positive bending. However, under negative bending since the compression flange is not supported by concrete slab, the girders with narrow flange

width show some sign of lateral torsional failure mode. Such failure modes were prevented by means of lateral restraint provided at the respective nodes and thus all girders exhibited post-peak deformations dominated by web shear postbuckling. In practice, the longitudinal girders are tied together by means of transverse girders or cross bracings spaced at predetermined interval thus reducing the buckling length.

## 5. Ultimate shear strength

An approximate method to predict the ultimate shear strength of the horizontally curved composite plate girders is presented in this section. The method is based on the technique proposed by Shanmugam and Baskar (2006) for the ultimate shear strength of straight composite plate girders. In this method, it is assumed that the ultimate shear carrying capacity of straight composite plate girders ( $V_{ult}$ ) may be obtained as sum of the shear carrying capacity of bare steel plate girder ( $V_s$ ) and contribution by concrete slab to the shear capacity ( $V_c$ ).

$$V_{ult} = V_s + V_c \quad (12)$$

It has been reported (Shanmugam and Baskar 2003) that tension field increases in width due to composite action between steel girder and concrete slab and, the final sway mechanism in the steel part of the composite girders is similar to the mechanism proposed for steel plate girders subjected to shear loading. Therefore, it is assumed that the tension field theory (Porter, *et al.* 1975, Evan, *et al.* 1978), for steel plate girders is applicable to obtain the shear capacity of the steel part of the composite plate girders. The diagonal tension field in the web of steel-concrete composite plate girder is partly anchored to the concrete slab through composite action and therefore, shear carrying capacity is enhanced. The extent of tension field anchored by the slab depends on the plastic hinge location, angle of inclination of the tension field, tensile strength of concrete, and the shear strength of concrete slab.

The tension field theory for straight steel plate girders (Porter, *et al.* 1975, Evan, *et al.* 1978) was, therefore, assumed herein to predict the shear capacity ( $V_s$ ) of the steel part of the composite girders. The value of  $V_s$  can be determined as

$$V_s = \tau_{cr} dt + \sigma_t^y t \sin^2 \theta (d \cot \theta - b) + 4 dt \sin \theta \sqrt{(\sigma_{yw} M_p^* \sigma_t^y)} \quad (13)$$

The details of the equation may be found elsewhere (Porter, *et al.* 1975, Evan, *et al.* 1978). The contribution by concrete slab to shear capacity of the girder is determined based on the assumed failure mechanism shown in Fig. 27. Composite action increases the load carrying capacity of the girder due to additional anchorage to the tension field.

The changes in the girder parameters such as location of plastic hinges and angle of inclination of tension field are accounted for in the proposed model. The contribution by the slab to shear carrying capacity of steel-concrete composite plate girder is given by

$$V_c = b_c \times T_l \times f_{ta} \quad (14)$$

in which,  $b_c$  is effective width of the slab,  $T_l$  anchor length (Fig. 27) and  $f_{ta}$  allowable split tensile stress of concrete. The value of ' $b_c$ ' may be taken as the effective width of concrete slab determined based on

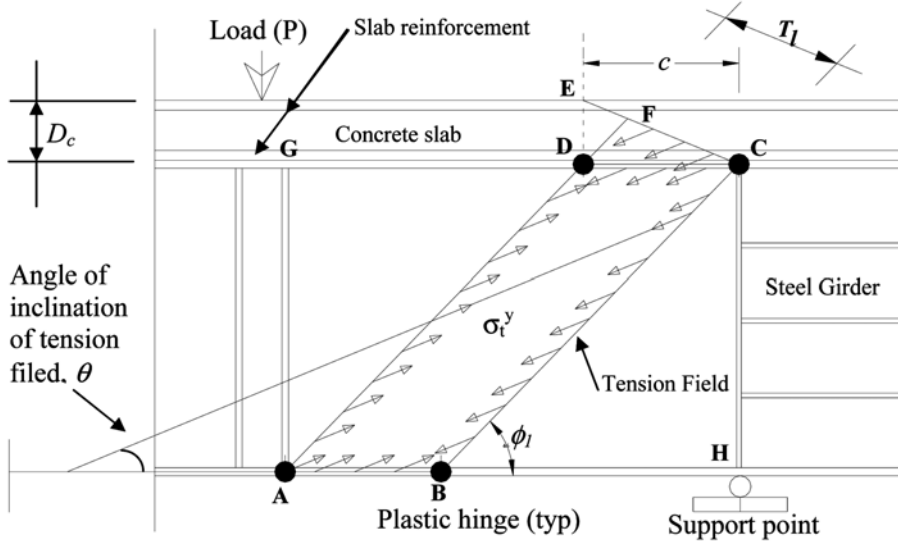


Fig. 27 Assumed failure mechanism for composite plate girders under shear loading

the code provisions. For an isolated composite girder such as those considered in the present study, the whole width of the slab may be assumed effective especially under shear loading. Further details of the mathematical model may be found elsewhere (Shanmugam and Baskar 2006).

The proposed method was applied to the horizontally curved composite girders with a modification factor ( $K_c$ ) to account for curvature of the girder. The modification factor,  $K_c$  for shear force was obtained by considering the bending of horizontally curved beam (Pytel and Singer 1987) shown in Fig. 28 as

$$K_c = \frac{3}{2\alpha} \left( \sin \alpha - \sin \frac{\alpha}{3} \right) \tag{15}$$

in which  $\alpha$  is half of the included angle at the centre of curvature. The curvature factor  $K_c$  can be used to

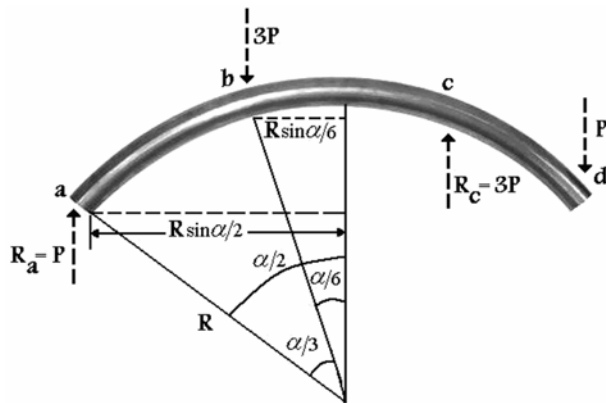


Fig. 28 Bending of horizontally curved beam

Table 1 Predicted and Finite element values of ultimate shear strength

Girder	b <sub>f</sub> mm	V <sub>c</sub> kN	V <sub>s</sub> kN	V <sub>ultpred</sub> kN	K <sub>c</sub> V <sub>ultpred</sub> kN	V <sub>ultFEA</sub>	V <sub>ultpred</sub> / V <sub>ultFEA</sub>
C <sub>1</sub>	203.3	565	1588	2153	1433	1419	1.01
	546.6	834	1801	2635	1754	1703	1.03
C <sub>1</sub> -C	203.3	798	1696	2494	1660	1643	1.01
	546.4	1007	1946	2953	1966	1927	1.02
C <sub>2</sub>	203.3	482	1503	1985	1317	1304	1.01
	557.3	681	1742	2423	1608	1546	1.04
C <sub>2</sub> -C	203.3	879	1677	2556	1696	1713	0.99
	556.3	952	1837	2789	1851	1833	1.01

obtain shear force at specified points along the curved girder based on the values corresponding to straight girders. The ultimate shear strength of a horizontally curved composite plate girder can thus be calculated as

$$V_{ult(curved)} = K_c (V_s + V_c) \quad (16)$$

The girders C<sub>1</sub>, C<sub>2</sub>, C<sub>1</sub>-C and C<sub>2</sub>-C considered in the previous section were assumed for ultimate shear strength calculations. Each of these girders was analyzed with two different flange widths viz. 203.3 mm and 546.6 mm/557.3 mm thus resulting in eight different girders. The straight girder values of  $V_s$ ,  $V_c$  and  $V_{ult}$  for the eight girders were determined first and the ultimate strength for the horizontally curved girders was obtained as  $V_{ultpred}$  equal to the product of  $V_{ult}$  and  $K_c$ . Shear strength values for the girders obtained from the analysis using LUSAS,  $V_{ultFEA}$  are listed along with  $V_{ultpred}$  in Table 1 for comparison. It can be seen from the table that there is close agreement between the finite element and predicted values, the maximum deviation being 4% thus confirming the accuracy of the proposed method. Despite the approximation, the proposed method is found to be capable of predicting the shear capacity of the horizontally curved composite plate girders to an acceptable accuracy. The method is simple and can readily be used at the preliminary stages of design.

## 6. Conclusions

The studies presented herein show that the elasto-plastic finite element code (LUSAS) employed is capable of predicting the elastic as well as ultimate load behaviour of steel-concrete composite plate girders with sufficient accuracy. The accuracy of the analyses is based on the comparison of the finite element results for steel girders and straight composite girders tested earlier by other researchers. Analyses using LUSAS have been carried out on composite plate girders curved in plan by varying radius of curvature, web panel widths and steel flange widths. It is apparent from the results that accounting for composite action between the concrete deck and steel section yields in larger load carrying capacity. Tension field action in web panels, similar to those observed in straight plate girders, is also observed in horizontally curved composite plate girders. It is concluded from the results presented herein that closely spaced transverse stiffeners which results in smaller web panel width enhances the shear resistance of the horizontally curved composite plate girders and hence the overall load carrying capacity. The increase in radius of curvature provides larger load carrying capacity i.e.

straight girders carry larger loads compared to the curved ones. It is obvious from the results that larger flange widths provide greater resistance to lateral bending besides giving larger moment capacity. An approximate method proposed herein has been shown to be capable of predicting the ultimate shear strength of horizontally curved composite plate girders with an acceptable level of accuracy.

## Acknowledgements

The authors are grateful for the support provided by the Department of Civil and Structural Engineering, Universiti Kebangsaan Malaysia.

## References

- AASHTO (2004), *LRFD bridge design specifications*, 3rd ed. 2005 Interim provisions, Washington (DC): American Association of State and Highway Transportation Officials.
- Allison, R.W., Johnson, R.P. and May, I.M. (1982), "Tension field action in composite plate girders", *Proc. of the Instn. of Civil Engrs*, London, **73**(2), 255-276.
- Baskar, K. and Shanmugam, N.E. (2003), "Steel-concrete Composite Plate Girders Subject to Combined Shear and Bending", *J. Constr. Steel Res.*, **59**(4), 531-557.
- Bradford, M.A., Uy, B. and Pi, Y.L. (2001), "Behaviour of unpropped composite girders curved in plan under construction loading", *Eng. Struct.*, **23**, 779-789.
- Evans, H.R., Porter, D.M. and Rockey, K.C. (1978), "The collapse behavior of plate girders subjected to shear and bending", *Int. Ass. Bridge Struct. Eng. periodical, proc.*, P-18/78.
- FEA Ltd. (2003), *LUSAS*, User Manual Version 13.7, Surrey, UK.
- Hall, D.H. (1996), "Curved girders are special", *Eng. Struct.*, **18**(10), 769-777.
- Jung, S.K. and White, D.W. (2006), "Shear strength of horizontally curved steel I girders finite element analysis studies", *J. Constr. Steel Res.*, **62**(4), 329-342.
- Lian, V.T. and Shanmugam, N.E. (2003), "Openings in Horizontally Curved Plate Girders", *Thin-Wall. Struct.*, **41**(2-3), 245-269.
- Lian, V.T. and Shanmugam, N.E. (2004), "Design of Horizontally Curved Plate Girder Webs Containing Circular Openings", *Thin-Wall. Struct.*, **42**(5), 719-739.
- Lääne, A. and Lebet, J.P. (2005), "Available rotation capacity of composite bridge plate girders under negative moment and shear", *J. Constr. Steel Res.*, **61**, 305327.
- Porter, D.M., Rockey, K.C. and Evans, H.R. (1975), "The collapse behavior of plate girders loaded in shear", *Struct. Eng.*, **53**(8), 313-325.
- Pytel, A. and Singer, F.L. (1987), *Strength of Materials*, 4th edition, Harpercollins College Div, New York.
- Shanmugam, N.E. and Baskar, K. (2003), "Steel-concrete Composite Plate Girders Subject to Shear loading", *J. Struct. Eng. ASCE*, **129**(9), 1230-1242.
- Shanmugam, N.E. and Baskar, K. (2006), "Design of Composite Plate Girders under Shear Loading", *Steel Compos. Struct.*, **6**(1), 1-14.
- Shanmugam, N.E., Mahendrakumar, M. and Thevendran, V. (2003), "Ultimate Load Behaviour of Horizontally Curved Plate Girders", *J. Constr. Steel Res.*, **49**(4), 509-529.
- Zureick, A.H., White, D.W., Phoawanich, N. and Park, J. (2002), "Shear strength of horizontally curved steel I girders-experimental tests", Final report to Professional Services Industries, Inc. and Federal Highway Administration.

**Notations**

$D$	: Depth of the plate girder
$f_c$	: Compressive strength of concrete
$f_t$	: Tensile strength of concrete
$\varepsilon_c$	: Compressive strain of concrete
$\varepsilon_t$	: Tensile strain of concrete
$t_w$	: Thickness of web
$b_f$	: Width of flange
$t_f$	: Thickness of flange
$L_b$	: Web panel length
$R$	: Radius of curvature
$P$	: Applied load
$V_n$	: Nominal shear resistance
$V_p$	: plastic shear force
$C$	: Ratio of the shear-buckling resistance to the shear yield strength
$k$	: Shear buckling coefficient
$V_{max}$	: Maximum shear force
$M_{max}$	: Maximum moment
$R_b$	: Strength reduction factor
$F_{yc}$	: Compression flange yield strength
$f_\ell$	: Elastically computed flange lateral bending stress
$S_{xc}$	: Elastic section modulus of the composite section to the compression flange
$\lambda_{rw}$	: Limiting slenderness ratio for a web
$b_s$	: Effective width of concrete deck,
$f_{DCI}$	: Compression flange stress at the section under consideration
$n$	: Modular ratio
$t_s$	: Thickness of concrete deck
$D_c$	: Depth of the web in compression in the elastic range.
$M_l$	: Flange lateral bending moment
$I_{yc}$	: Moment of inertia of the flanges about a vertical axis through the web
$AF$	: Amplification Factor
$C_m$	: Equivalent moment factor
$P_{ek}$	: Elastic buckling load.
$V_{ult}$	: Ultimate shear capacity of straight composite plate girders
$V_s$	: Shear carrying capacity of bare steel plate girder
$V_c$	: Shear capacity of concrete slab
$T_{cr}$	: Elastic buckling strength of web plate
$\sigma_i^y$	: Membrane stress acting over the tension band
$\theta$	: Angle of inclination of the tension field

- $\sigma_{yw}$  : Yield strength of web plate  
 $M_p$  : Flange parameters  
 $b_c$  : Effective width of the slab  
 $T_l$  : Anchor length  
 $f_{ta}$  : Allowable split tensile stress of concrete  
 $K_c$  : Modification factor  
 $\alpha$  : Half of the included angle at the centre of curvature